



Operating Quantum States in Single Magnetic Molecules: Implementation of Grover's Quantum Algorithm

C. Godfrin,^{1,2} A. Ferhat,^{1,2} R. Ballou,^{1,2} S. Klyatskaya,³ M. Ruben,³ W. Wernsdorfer,^{1,2,4,*} and F. Balestro^{1,2,5,†}

¹CNRS Institut Néel, Grenoble F-38000, France

²Université Grenoble Alpes, Institut NEEL, Grenoble F-38000, France

³Institute of Nanotechnology, Karlsruhe Institute of Technology, 76344 Eggenstein-Leopoldshafen, Germany

⁴Physikalisches Institut, Karlsruhe Institute of Technology, D-76131 Karlsruhe, Germany

⁵Institut Universitaire de France, 103 Boulevard Saint-Michel, 75005 Paris, France

(Received 17 July 2017; published 2 November 2017)

Quantum algorithms use the principles of quantum mechanics, such as, for example, quantum superposition, in order to solve particular problems outperforming standard computation. They are developed for cryptography, searching, optimization, simulation, and solving large systems of linear equations. Here, we implement Grover's quantum algorithm, proposed to find an element in an unsorted list, using a single nuclear $3/2$ spin carried by a Tb ion sitting in a single molecular magnet transistor. The coherent manipulation of this multilevel quantum system (qudit) is achieved by means of electric fields only. Grover's search algorithm is implemented by constructing a quantum database via a multilevel Hadamard gate. The Grover sequence then allows us to select each state. The presented method is of universal character and can be implemented in any multilevel quantum system with nonequal spaced energy levels, opening the way to novel quantum search algorithms.

DOI: 10.1103/PhysRevLett.119.187702

Introduction.—A quantum algorithm is a finite succession of unitary transformations performed on an initially prepared quantum state that aims to generate a final quantum state encoding the answer to a problem. The concept has attracted considerable attention after the discovery in 1994 by Shor describing that such an algorithm can factorize an integer with an exponentially smaller number of operations than any known classical algorithm [1]. A great deal of effort has been devoted since then to find new powerful quantum algorithms and to implement them in actual devices. Toward this goal, a variety of possible prototypes of a quantum bit (qubit) have been proposed [2–6] including nuclear spin systems [7–11], and experimental proofs of concept of quantum algorithms have been worked out [12–21]. A number of quantum algorithms have been formulated [22], among which one distinguishes those specifically simulating quantum systems, initially suggested by Feynman [23], and those relying on quantum Fourier transforms, such as Shor's algorithm for integer factorization [1]. The third main category of quantum algorithms incorporates the amplitude amplification discovered in 1997 by Grover to search an element in an unsorted list [24,25]. A few years later, a theoretical study proposed the implementation of this algorithm using a molecular magnet [26]. The Grover algorithm first creates an initial equal superposition of states by means of a Hadamard gate. Then it iteratively applies a quantum oracle to negate the amplitude of the searched state followed by a diffusion transform that inverts each amplitude about the average. Grover's algorithm was

proven to be quadratically faster than any classical search algorithm: After a number of iterations close to the square root of the length of the database, the final state collapses onto the searched state with a high probability. In previous experiments, the proof of concept of Grover's algorithm was demonstrated with nuclear magnetic resonance experiments on two [19,20] or three [21] entangled qubits, involving, respectively, four and eight states. A fundamentally different approach to the Grover algorithm was proposed in 1998 that does not make use of entangled qubits nor of a quantum oracle [27]. Instead, it was proposed to implement the algorithm into multilevel systems and to proceed by controlled time evolution of the wave functions of the different involved levels by driving Hamiltonians. Herein, we present the implementation of this approach using a single nuclear spin $I = 3/2$ [28]. After describing this four-level qudit, we present the coherent manipulation of each transition. Finally, the experimental implementation of the multilevel Grover algorithm is described consisting of two subsequent quantum gate operations: (i) A Hadamard gate creates the quantum directory by a coherent superposition of all the states, and (ii) the Hamiltonian of a unitary evolution will then make the system evolve to the desired state.

Reading out nuclear spin states.—All experimental results presented in this work were obtained via electric transport measurements through a three-terminal single-molecule magnet transistor. The device presented in Fig. 1(a) consists of a bis(phthalocyanine)terbium (III) single molecular magnet (SMM) (TbPc₂), contacted to two

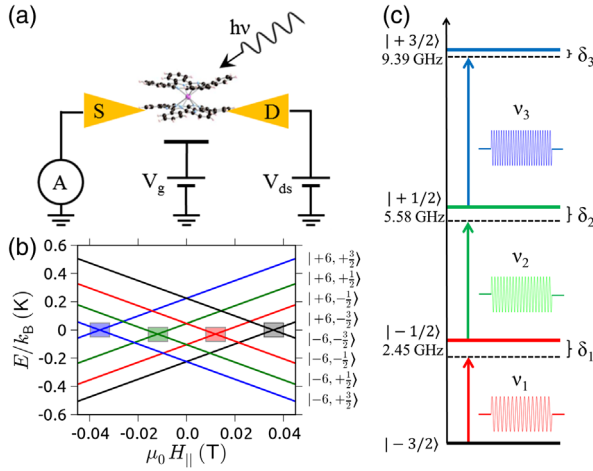


FIG. 1. (a) TbPc_2 molecular spin transistor schematic with source, drain, and gate electrodes: The Pc ligand connected to the source and drain is the readout quantum dot, allowing us to detect the nuclear spin state carried by the Tb^{3+} ion of TbPc_2 [11,31]. Microwave pulses allow a coherent manipulation of the nuclear spin carried by the ion via the ac Stark effect [32]. (b) Zeeman diagram of the molecule. The four colored squares indicate the anticrossing positions. By sweeping back and forth the magnetic field, a QTM is possible at these four positions. The electronic spin conductance dependence of the transistor enables us to read out the nuclear spin states. (c) Energy diagram of the four nuclear spin states. The quadrupole component in the hyperfine coupling enables an independent manipulation of each transition. We define the frequency of the microwave pulse ν_n that drives the $n-1 \leftrightarrow n$ transition and the detuning δ_n between the transition and microwave pulse frequency. Energy level values are taken for an external magnetic field $\mu_0 H_{\parallel} = -60$ mT. The color code from bottom to top is black for nuclear spin state $|-3/2\rangle$, red for $|-1/2\rangle$ and the transition from $|-3/2\rangle$ to $|-1/2\rangle$, green for $|1/2\rangle$ and the transition from $|-1/2\rangle$ to $|1/2\rangle$, and blue for $|3/2\rangle$ and the transition from $|1/2\rangle$ to $|3/2\rangle$.

gold electrodes by using the electromigration technique [29]. The heart of the molecule is a Tb^{3+} ion that is eightfold coordinated by two phthalocyanine (Pc) ligands. It exhibits an electronic configuration $[\text{Xe}]4f^8$ with a total spin $S = 3$ and a total orbital momentum $L = 3$. A strong spin-orbit coupling yields an electronic ground state spin with a total angular magnetic moment $J = 6$. In addition, the ligand field generated by the two Pc ligands lifts the degeneracy of the $J = 6$ multiplet, leading to an energy gap of the order of 600 K from the ground state doublet $m_j = \pm 6$ compared to $m_j = \pm 5$. Because the measurements are performed at a very low temperature (electron temperature $T_{\text{el}} = 50$ mK), the electronic spin can be considered as a ± 6 Ising spin with a uniaxial anisotropy axis perpendicular to the Pc plane [Fig. 1(a)]. In addition to the electronic spin, the monoisotopic $^{159}\text{Tb}^{3+}$ ion carries a nuclear spin $I = 3/2$. The hyperfine interaction of $A \approx 24.9$ mK [30] between the electronic and the nuclear spin results in a fourfold level splitting of each electronic spin state as presented in the Zeeman diagram [Fig. 1(b)]. The quadrupole term

$P \approx 14.4$ mK of the hyperfine coupling yields an unequal energy level spacing between the four nuclear spin states, resulting in three different resonance frequencies $\nu_1 \approx 2.45$ GHz, $\nu_2 \approx 3.13$ GHz, and $\nu_3 \approx 3.81$ GHz [Fig. 1(c)]. Off-diagonal terms in the ligand-field Hamiltonian give rise to a finite tunnel probability from one electronic spin state into the other, conserving the nuclear spin state. The colored rectangles in Fig. 1(b) indicate the position of the avoided level crossings where quantum tunneling of the magnetization (QTM) can occur. We previously reported that the magnetic moment of both the single electronic and nuclear spin can be read out via transport measurements [11,31] and that the coherent manipulation of a single nuclear spin can be performed using electric fields only [32]. In solid state devices, the readout and coherent manipulation of a nuclear spin was also achieved for nitrogen-vacancy centers in diamond [9] and an ionized ^{31}P donor in silicon [10].

The SMM transistor is cooled down using a dilution refrigerator. Using a 3D vector magnet, magnetic fields $\mu_0 H_{\parallel}$ parallel to the easy axis of the TbPc_2 are applied. Microwave pulses of frequency ν_{rf} , amplitude E_{rf} , and duration τ_{rf} are applied via an antenna in the vicinity of the device using two different microwave setups detailed in Supplemental Material [33]. For Rabi (Fig. 2), Ramsey, and Hahn echo experiments (see [33]), we used a monochromatic pulse synthesized by a Rhode & Schwarz SMA100A generator with an arbitrary wave generator (AWG) external pulse modulation. To perform Hadamard gates and demonstrate the Grover algorithm implementation, we used a Tektronix AWG 7122B to synthesize the pulse sequences point by point. Initialization, coherent manipulation, and readout of the single nuclear spin use the following cycle: First, the external magnetic field is swept from +60 to -60 mT at 100 mT/s [Fig. 1(b)]. If a QTM transition is measured, depending on the field value at which it occurs, the respective nuclear spin state can be accessed. Second, at a constant external magnetic field $\mu_0 H_{\parallel} = -60$ mT, a microwave electrical pulse is applied. Through the ac Stark effect, the hyperfine interaction A is ac modulated. As a result, the nuclear spin undergoes an ac effective magnetic field with amplitude B_{eff} up to 300 mT [32]. Finally, the resulting state is detected by sweeping back the external magnetic field from -60 to +60 mT at 100 mT/s. As a QTM event depends on the Landau Zener probability [35–37], the entire sequence is rejected when no QTM transition is detected. After repeating this procedure 1000 times for each pulse sequence, we yield the transition probability between the nuclear states i and j :

$$P_{i,j} = \frac{N_{i,j}}{\sum_n N_{i,n}}, \quad (1)$$

where $N_{i,j}$ is the number of events of initial state i and final states j . First, we study each nuclear spin transition separately. The transition Hamiltonian in the rotating frame is given by

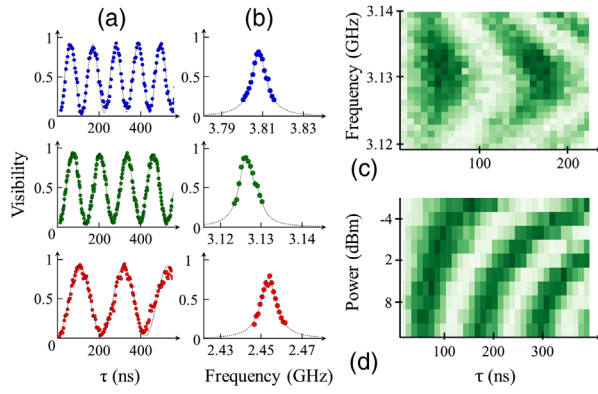


FIG. 2. (a) Rabi oscillations: The frequency of the oscillations can be tuned from 1.5 to 8 MHz (see [33]). Each color represents a qubit transition: from bottom to top, transitions 1, 2, and 3, respectively, in red, green, and blue. (b) By recording the maximum of visibility of the Rabi oscillation as a function of the detuning, we measure the resonance shape of the three transitions. (c) Visibility of the second state as a function of the pulse length and frequency. The detuning increases the frequency of the oscillation and decreases the maximum of visibility. (d) Visibility of the second state as a function of the pulse length and power. A linear dependence of the Rabi frequency as a function of the square root of the pulse power is measured.

$$H_{\text{qubit}} = \pi\hbar(\delta\sigma_z + \Omega\sigma_x) = \pi\hbar \begin{pmatrix} \delta & \Omega \\ \Omega & -\delta \end{pmatrix}, \quad (2)$$

where σ_k are the Pauli matrices, $\delta = \nu_{qb} - \nu_{rf}$ is the detuning between the pulse and the spin transition, and $\Omega = g\mu_N B_{\text{eff}}/\hbar$ is the Rabi frequency. At resonance ($\delta = 0$), the state of the qubit will rotate around the x axis of the Bloch sphere at the frequency Ω , resulting in a coherent oscillation between the population of the two states of the qubit. The visibility, defined as $V_{ij} = P_{i,j} + P_{j,i}$, as a function of the pulse length for the three frequencies of the nuclear spin state ($\nu_1 = 2.452$ GHz, $\nu_2 = 3.128$ GHz, and $\nu_3 = 3.799$ GHz), is displayed in Fig. 2(a). These oscillations exhibit a high-fidelity coherent control of each nuclear spin transitions. As presented in Fig. 2(d) and in detail in Ref. [33], the Rabi frequency fits linearly with the microwave amplitude, as theoretically predicted. The detuning can also be adjusted by pitching the microwave pulse frequency. As shown in Figs. 2(b) and 2(c), the higher the detuning, the lower the oscillation visibility and the higher the oscillation frequency. These results show that the molecular magnet single nuclear spin transistor geometry is a three-qubit system, where all the dynamic parameters can be tuned. Furthermore, we measured coherence times of the order of a millisecond (see [33]), which allow us to make more than a thousand coherent spin manipulations before decoherence processes set in.

Grover algorithm implementation.—In order to benefit from quantum parallelism and to implement Grover's research algorithm, the different transitions were driven simultaneously using a multichromatic microwave pulse.

We make use of the generalized rotating frame [28] to treat the interaction of a multilevel system with a multichromatic pulse. Making the assumption of a near-resonance condition for each pulse frequency and the rotating wave approximation, the Hamiltonian H_{qd} of a four-state qudit system driven by a pulse composed of three frequencies is

$$H_{qd} = \pi\hbar \begin{pmatrix} 0 & \Omega_1 & 0 & 0 \\ \Omega_1 & 2\delta_1 & \Omega_2 & 0 \\ 0 & \Omega_2 & 2\delta_2 & \Omega_3 \\ 0 & 0 & \Omega_3 & 2\delta_3 \end{pmatrix}, \quad (3)$$

where δ_n and Ω_n are, respectively, the frequency detuning and the Rabi frequency of the n th transition. In this frame, the Hamiltonian is time independent. All unitary operations can be described via the evolution operator:

$$U = e^{-iH_{qd}t/\hbar}. \quad (4)$$

The first gate of Grover's algorithm, the Hadamard gate, creates a quantum database, i.e., prepares the system in a coherent superposition of all the nuclear spin states:

$$|\Psi(\tau)\rangle = U(\tau)|\Psi_i\rangle = \frac{1}{\sqrt{N}} \sum_{n=0}^{N-1} |n\rangle, \quad (5)$$

where τ is the pulse length that creates the superposition and $|\Psi_i\rangle$ the initial state. In the generalized rotating frame formalism, it is mandatory to find a combination of $2N - 1$ parameters ($N - 1$ for Ω_n , $N - 1$ for δ_n , and the evolution time) that satisfies this equation. Note that both the phase and population of all states must be equal. Parameters were obtained using a variance minimization simulation of the population and phase. The desired pulse was synthesized point by point using a 24 GS/s AWG.

In this section, the visibility is defined as $V_{i,j} = P_{i,j}$. First, starting from the initial state $|+1/2\rangle$, we applied the Hadamard gate to states $|+1/2\rangle$ and $|-1/2\rangle$ yielding a two-state coherent superposition. Whereas a $\pi/2$ pulse creates a superposition of two states with a phase difference of π , the Hadamard gate with a detuning equal to the transition rate ($\delta = \Omega$) ensures a state population and phase equality. As shown in Fig. 3(a), this is obtained starting from the $|+1/2\rangle$ state and driving the second transition with the set of parameter $\delta_2 = \Omega_2 = 3.1$ MHz and a pulse length of 115 ns. Next, a three-state coherent superposition is presented in Fig. 3(b), starting from the $|-1/2\rangle$ state and driving the first and second transitions, using $\delta_1 = \Omega_1 = \Omega_2 = 2.4$ MHz. Because of the Hamiltonian's symmetry, the $|-3/2\rangle$ and the $|+1/2\rangle$ state have the same dynamics. Finally, for the four-state superposition, we started with the $|+1/2\rangle$ state. The set of parameters

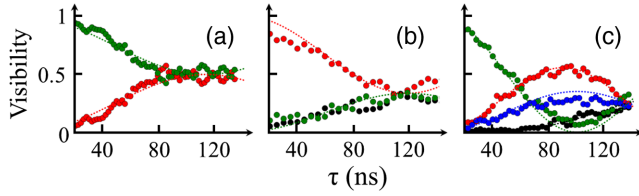


FIG. 3. Evolution of the nuclear spin state population as a function of the microwave pulse length. The color code is the same as used for Fig. 1. From left to right, we show that we are able to create coherent superposition of two, three, and four single nuclear spin states. For the two- (a) and three-state (b) superpositions, we choose experimental parameters that ensure the same phase for all the states when they have the same population, leading to the so-called Hadamard gate.

$\delta_1 = \delta_2 = \delta_3 = 0$; $\Omega_1 = 2.1$ MHz; $\Omega_2 = 4.2$ MHz; $\Omega_3 = 3.1$ MHz yielded a coherent superposition with a pulse length of 140 ns [Fig. 3(c)]. However, for this coherent superposition, each state has a different phase.

These measurements show that this system can be used as a four-state quantum directory. The second gate of Grover's algorithm is used to amplify the population of a researched state. This can be achieved by creating a resonant condition in between the superposed state and the researched state. Under this condition, the system will oscillate between these two states and, after a half period of oscillation, will be in the researched state. Note that this unitary evolution has a \sqrt{N} dependence of the period:

$$\tau = \frac{\sqrt{N}}{4\Omega} \quad (6)$$

as detailed in Ref. [33]. Experimentally, this resonant condition is obtained by applying a specific energy to the researched state. In the rotating frame, this means a specific detuning. In the general case of an N -element database, the resonant condition is

$$\langle s|H_{qd}|s\rangle = \frac{1}{N} \sum_{n,m} \langle m|H_{qd}|n\rangle, \quad (7)$$

where $|s\rangle$ is the researched state. For three states, this expression leads to

$$\delta_s = \frac{\Omega_1 + \Omega_2 + \delta_1 + \delta_2}{3}. \quad (8)$$

If we apply a detuning only to the researched state, the condition is

$$\delta_s = \frac{\Omega_1 + \Omega_2}{2}. \quad (9)$$

In order to synthesize the microwave pulse sequence with amplitude and phase control, we use a 24 GS/s AWG. Starting from the $|-1/2\rangle$ state, the Hadamard gate is first applied to create the three-state coherent superposition as

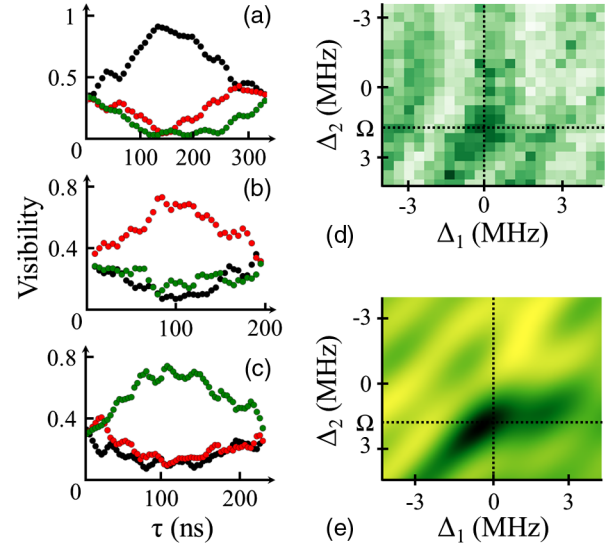


FIG. 4. Grover evolution. Dynamic of the population in a function of the unitary evolution pulse length. Starting from a superposed three states [see Fig. 3(b)], obtained using a Hadamard gate, we show that we are able to create an oscillation between this superposed state and a desired state. Depending on the detuning we choose to apply in this sequence, the population from either the black $|-3/2\rangle$ (a), the red $|-1/2\rangle$ (b), or the green $|+1/2\rangle$ (c) state increases. The Hadamard gate followed by this unitary evolution represents the implementation of Grover's algorithm. Experimental (d) and theoretical (e) visibility as a function of the two pulse frequencies at a fixed pulse duration. The visibility is maximized when the resonant condition is satisfied.

presented in Fig. 3(b). Then, the second pulse is generated with the same power (same Ω) but with a modification of the frequency in order to satisfy the resonant condition. The pulse parameters ($-\delta_1 = -\delta_2 = \Omega_1 = \Omega_2 = 3.4$ MHz) select the $|-3/2\rangle$ state, ($\delta_1 = \Omega_1 = \Omega_2 = 3.0$ MHz) the $|-1/2\rangle$ state, and ($\delta_2 = \Omega_1 = \Omega_2 = 4.9$ MHz) the $|+1/2\rangle$ state [Figs. 4(a)–4(c), respectively]. In all the cases, the population of the nuclear spin is clearly in the researched states (respectively, a visibility of 0.9, 0.7, and 0.75). In order to underline the resonant character of this algorithm, we present a map of the visibility of the $|+1/2\rangle$ state as a function of the two frequencies that composed the pulse for a constant pulse length corresponding to the half-Grover period [Fig. 4(d)]. As expected, the visibility is maximized when the resonant condition is reached ($\delta_1 = 0$ MHz and $\delta_2 = \Omega_1 = \Omega_2 = 4.9$ MHz). The experimental map compares well with the simulation obtained using the generalized rotating frame [Fig. 4(e)], demonstrating the implementation of the Grover search algorithm obtained using the resonance between a single state and a three superposed state of a single nuclear spin.

These results show how the coherent control over a single nuclear spin embedded in a molecular spin transistor can be gained and read out nondestructively. It leads to the first experimental implementation of Grover's algorithm

using a multilevel system. The presented two-step quantum operation can be extended to be performed on alternative spin qubit devices. The great diversity of available molecular magnets with their inherent tunability will potentially provide higher nuclear spin values that might make accessible much bigger databases for the field of molecular quantum computation.

We gratefully acknowledge E. Eyraud, D. Lepoittevin, and C. Hoarau for their technical contributions, T. Fournier, T. Crozes, B. Fernandez, S. Dufresnes, and G. Julie for nanofabrication development, E. Bonet and C. Thirion for help with software development, and R. Vincent and S. Thiele for the development of the experiment. Samples were fabricated in the NANOFAB facility of the Néel Institute. This work is partially supported by ANR-13-BS10-0001 MolQuSpin. This work has been partially supported by the European Community through the FET-Proactive Project MoQuaS (Contract No. 610449), by the German Research Foundation (DFG) through the Transregio Project No. TR88 3MET, and by the Alexander von Humboldt Foundation.

* wolfgang.wernsdorfer@kit.edu

† franck.balestro@neel.cnrs.fr

- [1] P. W. Shor, in *Proceedings of the 35th Annual Symposium on Foundations of Computer Science*, edited by S. Goldwasser (IEEE, Los Alamitos, 1994).
- [2] C. Monroe, D. Meekhof, B. King, and D. A. Wineland, *Science* **272**, 1131 (1996).
- [3] M. Brune, F. Schmidt-Kaler, A. Maali, J. Dreyer, E. Hagley, J. M. Raimond, and S. Haroche, *Phys. Rev. Lett.* **76**, 1800 (1996).
- [4] Y. Nakamura, Y. A. Pashkin, and J. Tsai, *Nature (London)* **398**, 786 (1999).
- [5] D. Kim *et al.*, *Nat. Nanotechnol.* **10**, 243 (2015).
- [6] F. Jelezko, T. Gaebel, I. Popa, A. Gruber, and J. Wrachtrup, *Phys. Rev. Lett.* **92**, 076401 (2004).
- [7] B. E. Kane, *Nature (London)* **393**, 133 (1998).
- [8] M. G. Dutt, L. Childress, L. Jiang, E. Togan, J. Maze, F. Jelezko, A. S. Zibrov, P. R. Hemmer, and M. D. Lukin, *Science* **316**, 1312 (2007).
- [9] P. Neumann, J. Beck, M. Steiner, F. Rempp, H. Fedder, P. R. Hemmer, J. Wrachtrup, and F. Jelezko, *Science* **329**, 542 (2010).
- [10] J. J. Pla, K. Y. Tan, J. P. Dehollain, W. H. Lim, J. J. Morton, F. A. Zwanenburg, D. N. Jamieson, A. S. Dzurak, and A. Morello, *Nature (London)* **496**, 334 (2013).
- [11] R. Vincent, S. Klyatskaya, M. Ruben, W. Wernsdorfer, and F. Balestro, *Nature (London)* **488**, 357 (2012).
- [12] C. Y. Lu, D. E. Browne, T. Yang, and J. W. Pan, *Phys. Rev. Lett.* **99**, 250504 (2007).
- [13] B. P. Lanyon, T. J. Weinhold, N. K. Langford, M. Barbieri, D. F. V. James, A. Gilchrist, and A. G. White, *Phys. Rev. Lett.* **99**, 250505 (2007).
- [14] A. Politi, J. Matthews, and J. O'Brien, *Science* **325**, 1221 (2009).
- [15] E. Martin-Lopez, A. Laing, T. Lawson, R. Alvarez, X. Q. Zhou, and J. L. O'Brien, *Nat. Photonics* **6**, 773 (2012).
- [16] X.-D. Cai, C. Weedbrook, Z.-E. Su, M.-C. Chen, Mile Gu, M.-J. Zhu, L. Li, N.-L. Liu, C.-Y. Lu, and J.-W. Pan, *Phys. Rev. Lett.* **110**, 230501 (2013).
- [17] S. Barz, I. Kassal, M. Ringbauer, Y. O. Lipp, B. Dakic, A. Aspuru-Guzik, and P. Walther, *Sci. Rep.* **4**, 6115 (2014).
- [18] J. King, S. Yarkoni, M. M. Nevisi, J. P. Hilton, and C. C. McGeoch, *arXiv:1508.05087*.
- [19] J. A. Jones, M. Mosca, and R. H. Hansen, *Nature (London)* **393**, 344 (1998).
- [20] I. L. Chuang, N. Gershenfeld, and M. Kubinec, *Phys. Rev. Lett.* **80**, 3408 (1998).
- [21] L. M. Vandersypen, M. Steffen, M. H. Sherwood, C. S. Yannoni, G. Breyta, and I. L. Chuang, *Appl. Phys. Lett.* **76**, 646 (2000).
- [22] S. Jordan, <http://math.nist.gov/quantum/zoo/>.
- [23] R. Feynman, *Int. J. Theor. Phys.* **21**, 467 (1982).
- [24] L. K. Grover, in *Proceedings of the 28th Annual ACM Symposium on Theory of Computing (STOC, Philadelphia PA, USA, 1996)*, pp. 212–219.
- [25] L. K. Grover, *Phys. Rev. Lett.* **79**, 325 (1997).
- [26] M. N. Leuenberger and D. Loss, *Nature (London)* **410**, 789 (2001).
- [27] E. Farhi and S. Gutmann, *Phys. Rev. A* **57**, 2403 (1998).
- [28] M. N. Leuenberger and D. Loss, *Phys. Rev. B* **68**, 165317 (2003).
- [29] H. Park, J. Park, A. K. Lim, and E. H. Anderson, *Nature (London)* **407**, 57 (2000).
- [30] N. Ishikawa, M. Sugita, and W. Wernsdorfer, *Angew. Chem., Int. Ed. Engl.* **44**, 2931 (2005).
- [31] C. Godfrin, S. Thiele, K. Ferhat, S. Klyatskaya, M. Ruben, W. Wernsdorfer, and F. Balestro, *ACS Nano* **11**, 3984 (2017).
- [32] S. Thiele, F. Balestro, R. Ballou, S. Klyatskaya, M. Ruben, and W. Wernsdorfer, *Science* **344**, 1135 (2014).
- [33] See Supplemental Material at <http://link.aps.org/supplemental/10.1103/PhysRevLett.119.187702> for additional information on the experimental setup and on the coherent manipulation of a multilevel system, which includes Refs. [11,27,28,31,34].
- [34] M. Martens, J. van Tol, N. S. Dalal, S. Bertaina, and I. Chiorescu, *arXiv:1505.03177*.
- [35] L. D. Landau, Zur theorie der energieübertragung. II. *Phys. Z. Sowjetunion* **2**, 1 (1932).
- [36] C. Zener, *Proc. R. Soc. A* **137**, 696 (1932).
- [37] F. Troiani, C. Godfrin, S. Thiele, F. Balestro, W. Wernsdorfer, S. Klyatskaya, M. Ruben, and M. Affronte, *Phys. Rev. Lett.* **118**, 257701 (2017).